Dalton Transactions

A Higher Voltage Fe(II) Bipyridine Complex for Non-Aqueous Redox Flow Batteries

Journal:	*Dalton Transactions*
Manuscript ID	DT-ART-11-2020-003927
Article Type:	Paper
Date Submitted by the Author:	16-Nov-2020
Complete List of Authors:	Cammack, Claudina; Sandia National Laboratories, Power Sources Pratt III, Harry; Sandia National Laboratories, Power Sources Small, Leo; Sandia National Laboratories, Nanoscale Sciences Dept. Anderson, Travis; Sandia National Laboratories, Power Sources Technology Group

A Higher Voltage Fe(II) Bipyridine Complex for Non-Aqueous Redox Flow Batteries

Claudina X. Cammack,[a] Harry D. Pratt III, [a] Leo J. Small,[a] and Travis M. Anderson [*a]

[a]Sandia National Laboratories, Albuquerque, New Mexico, 87185-00613, USA

*Email: tmander@sandia.gov

Electronic Supplementary Information (ESI) Available

Abstract

Non-aqueous redox flow batteries (RFBs) offer the possibility of higher voltage and a wider working temperature range than their aqueous counterpart. Here, we optimize the established 2.26 V $Fe(bpy)_3(BF_4)_2$/$Ni(bpy)_3(BF_4)_2$ asymmetric RFB to lessen capacity fade and improve energy efficiency over 20 cycles. We also prepared a family of substituted $Fe(bpyR)_3(BF_4)_2$ complexes (R= -CF_3, -CO_2Me, -Br, -H, -^{t}Bu, -Me, -OMe, -NH_2) to potentially achieve a higher voltage RFB by systematically tuning the redox potential of $Fe(bpyR)_3(BF_4)_2$, from 0.94 V vs. Ag/AgCl for R = OMe to 1.65 V vs. Ag/AgCl for R = CF_3 (ΔV = 0.7 V). A series of electronically diverse symmetric and asymmetric RFBs were compared and contrasted to study electroactive species stability and efficiency, in which the unsubstituted $Fe(bpy)_3(BF_4)_2$ exhibited the highest stability as a catholyte in both symmetric and asymmetric cells with voltage and Coulombic efficiencies of 94.0% and 96.5%, and 90.7% and 80.7%, respectively.

Introduction

Redox flow batteries (RFBs) show promise as a flexible and efficient option for large-scale energy storage systems (ESS) due to their low cost, safety, and long cycle life.[1,2] Their unique configuration consisting of liquid electrolyte-containing reservoirs offer RFBs the advantage of decoupling energy and power densities. This characteristic allows flow batteries to easily be scaled up for greater energy by increasing the reservoir size of working electrolyte.[3,4] While aqueous RFBs are well-established and commercially available, non-aqueous RFBs are still in the early stages of development but have the potential to overcome the less than 1.5 V electrochemical window of water.[5,6]

A common obstacle in designing a high-performance RFB is maintaining charge balance in the electrochemical cell as the battery operates, while minimizing active species crossover of the anolyte and catholyte. Crossover has shown to be a central issue in many non-aqueous RFBs which is detrimental to battery health and results in self-discharge and permanent loss of battery capacity.[7] A root cause of crossover is lack of non-aqueous flow battery membranes, as most commonly employed ion exchange membranes utilized in RFBs were designed for aqueous applications such as desalination and electrodialysis.[8] Because research to produce a high performance non-aqueous membrane is still ongoing,[9] design of a symmetric RFB consisting of a single molecule as both the anolyte and catholyte has been used to counter crossover. Cell rebalancing due to chemical crossover no longer requires chemical separation when the active species are the same, thus restoring battery capacity.[10] Construction of a symmetric system requires a molecule having accessible and stable redox potentials that are also separated by a wide voltage window that serves as the battery voltage. Energy density is known to be related to voltage, concentration, and the number of electrons transferred in a redox event, given by,

$$E_{vol} = 1/2nV_{cell}FC_{active}$$

where n is the number of electrons transferred, V_{cell} is the cell voltage, F is Faraday's constant, and C_{active} is the concentration of active species. We chose to focus this manuscript on improved battery voltage.

Redox-active molecules that meet the requirements listed above can be attained through molecular tuning, and synthetic inorganic chemistry offers advantages for the design of high-performance, symmetric, non-aqueous RFBs. Metal coordination complexes (MCCs) naturally have higher solubility in organic solvents of similar polarity than ionic metal salts due to chelation with soluble organic ligands. Because organic solvents make higher voltage batteries attainable, thoughtful ligand design coupled with electrochemically active transition metals can be exploited to produce a battery with higher energy and power density, all due to better solubility. MCCs have been employed as electroactive species in non-aqueous RFBs due to their ease of tunability and the excellent redox properties of transition metals. Early work by Anderson *et al.* focused on the synthesis of MCC ionic liquids to achieve high energy density, but were limited by low voltages (< 2 V).[11,12] In the past 5 years, metals across the *d*-block have been used in complexes with innocent and non-innocent ligands, including ligands of varying denticity. Of the traditional

ligands, acetylacetone (acac) is widely used and found in both symmetric and asymmetric cells in V, Cr, Fe, Mn, and Ru complexes.[13,14,15,16,17] Of the metal-acac complexes studied, an all-iron system containing $Fe(acac)_3$ as the anolyte achieved high Coulombic, voltage, and energy efficiencies over 100 cycles.[14] Nitrogen-donating ligands are commonly employed in MCCs for their affinity to various transition metals and formation of often stable complexes. Some nitrogen-donating MCCs include nickel picolinamide as an anolyte,[18] a nickel-cyclam complex that achieved a cell voltage of 2.55 V,[19] dithiolene complexes of V, Fe, Co, Ni, and Cu,[20] a family of Co-azole-pyridine complexes,[21] and multi-electron redox-active tridentate bipyridylimino isoindoline complexes (BPI) of Mg, Mn, Fe, Co, Ni, and Zn in which Ni(BPI) exhibited the highest stability and solubility for use as an anolyte in non-aqueous RFBs. Nitrogen-containing ligands of relevance to this work are the polypyridyl ligands phenanthroline (phen), terpyridine (terpy), and bipyridine (bpy). While these ligands are mainstays in coordination chemistry, their application in RFBs has been limited. The 2019 review by Hogue and Toghill well summarizes MCCs in non-aqueous RFBs.[22] Other metal-containing compounds have been explored for RFBs but will not be discussed here.‡

Seminal work by Mun *et al.* on an $Fe(bpy)_3(BF_4)_2$/$Ni(bpy)_3(BF_4)_2$ (**Samsung 1**) non-aqueous RFB showed the feasibility of producing a 2.25 V cell potential with highly stable half-cell reactions.[23] The system exhibited promising charge-discharge cycles with 90.4% Coulombic efficiency and 81.8% energy efficiency, respectively. Coulombic efficiency (CE) is the ratio of discharge time to charge time, and voltage efficiency (EE) is the average discharge voltage divided by the average charge voltage. Energy efficiency (EE) is the product of Coulombic and voltage efficiencies. This **Samsung 1** system was the inspiration for an exhaustive study on membranes due to the high ion crossover observed for the system.[24] Mun *et al*. improved their **Samsung 1** system by creating **Samsung 2**, a symmetric RFB to prevent anolyte crossover and increase energy density using $Fe(bpy)_3(TFSI)_2$ in $TEABF_4$/PC (TFSI = bis(trifluoromethylsulfonyl)imide).[25] Exchange of the BF_4^- counterion for $TFSI^-$ showed increased solubility due to decreased dissociation energy but decreased conductivity as a result of the $TFSI^-$ bulkiness. Our system builds upon **Samsung 1** and **2** chemistries and employs classical coordination chemistry to tune the electrochemical properties of these complexes.

Abundant and cost effective, easily synthesized iron complexes exhibit reversible and tunable Fe^{2+}/Fe^{3+} redox couples. RFBs using transition metal-bipyridyl complexes as the working electrolytes show

electrochemical stability and solubility in various charge states and multiple solvents.[17,18] Coordination of Fe^{2+} with N-heterocyclic chelating ligands such as bpy form stable metal complexes through the chelate effect, the strong σ-donating and π-accepting properties of bpy, and the good π-donating abilities of Fe^{2+} to ligands with low-lying π* orbitals. Furthermore, the electrochemical non-innocence of bpy makes multiple redox events accessible in addition to the metal centered $Fe^{2+/3+}$ couple. In order for an Fe-bpy coordination complex to be effective as both positive and negative RFB electroactive species, metal-centered and ligand-centered redox events must be separated and accessible under flow battery conditions. Here we present the optimization of Samsung chemistries and the synthesis and characterization of a family of $Fe(bpyR)_3(BF_4)_2$ complexes for application in symmetric, non-aqueous RFBs with a high working voltage, high efficiency, and low electrolyte crossover.

Experimental

4,4'-di(trifluoromethane)-2,2'-bipyridine ($bpyCF_3$), 4,4'-dibromo-2,2'-bipyridine (bpyBr), 4,4'-di(tert-butyl)-2,2'-bipyridine (bpy^tBu), 4,4'-dimethyl-2,2'-bipyridine (bpyMe), 4,4'-dimethoxy-2,2'-bipyridine (bpyOMe), bipyridine (bpy), iron(II) tetrafluoroborate hexahydrate ($Fe(BF_4)_2{\cdot}6H_2O$), tetraethylammonium tetrafluoroborate ($TEABF_4$), tetrabutylammonium tetrafluoroborate ($TBABF_4$), tetrabutylammonium hexafluorophosphate ($TBAPF_6$), tetrabutylammonium trifluoromethanesulfonate (TBAOTf), tetrabutylammonium and bis(trifluoromethane)sulfonimide (TBATFSI), were used as purchased from Sigma-Aldrich or Strem Chemicals. Battery-grade propylene carbonate was used as purchased from Chameleon Reagents. Ligands 4,4'-dicarboxy-2,2'-bipyridine ($bpyCO_2Me$)[26] and 4,4'-diamino-2,2'-bipyridine ($bpyNH_2$)[27] were prepared according to literature procedures. Multinuclear NMR measurements were collected on a Bruker AVANCE III 500 and referenced to residual solvent signal. UV-Vis spectroscopy was performed on an Agilent Cary 5000 UV-Vis-NIR spectrophotometer. Infrared spectra were recorded on a Thermo Fisher Nicolet iS5 FT-IR equipped with a Smart Orbit ATR accessory. MALDI-MS was performed with a Waters Corporation QTOF mass spectrometer model G2 and various mass ranges were collected in positive mode.

General procedure for the synthesis of Fe(4,4'-diR-2,2'-bipyridiyl)$_3$(BF$_4$)$_2$:

The appropriate 4,4'-diR-2,2'-bipyridine (3 equiv.) was combined with Fe(BF$_4$)$_2$·6H$_2$O (1 equiv.) in the minimum amount of methanol needed to dissolve the reactants. The resulting blood-red solution was stirred at room temperature overnight, filtered and washed with methanol, and the filtrate was concentrated under reduced pressure.

Fe(bpy)$_3$(BF$_4$)$_2$: Yield: 77% (13.5 g). ^{1}H NMR (500 MHz, DMSO-d_6): δ 8.86 (d, *J* = 8.1 Hz, 6H), 8.23 (td, *J* = 7.8, 1.6 Hz, 6H), 7.56-7.50 (m, 6H), 7.39 (d, *J* = 4.1 Hz, 5H). ^{13}C NMR (125 MHz, acetone-d_6): δ 160.49, 155.37, 139.99, 128.76, 125.20. IR (ν, cm^{-1}): 1604, 1443, 1030, 770. UV-Vis absorption: λ (nm), ε (M^{-1}cm^{-1}): 246(28100), 298(63800), 250(6100), 482(sh, 6700), 522(8100).

Fe(bpyCF$_3$)$_3$(BF$_4$)$_2$: Yield: 95% (3.6 g). ^{1}H NMR (500 MHz, DMSO-d_6): δ 9.01 (d, *J* = 5.0 Hz, 6H), 8.61 (s, 6H), 7.93 (d, *J* = 5.1 Hz, 6H). ^{13}C NMR (125 MHz, DMSO-d_6): δ 153.64, 149.85, 136.66, 118.99, 114.32, 29.15. IR (ν, cm^{-1}): 1413, 13229, 1269, 1135, 1049, 840. UV-Vis absorption: λ (nm), ε (M^{-1}cm^{-1}): 239(30800), 295(44000), 361(4200), 491 (sh, 4000), 530(5300).

Fe(bpyCO$_2$Me)$_3$(BF$_4$)$_2$: Yield: 88% (558 mg). ^{1}H NMR (500 MHz, MeOH-d_4): δ 9.24 (s, 6H), 7.95 (d, *J* = 4.9 Hz, 6H), 7.71 (d, *J* = 6.1 Hz, 6H), 4.04 (s, 18H). ^{13}C NMR (125 MHz, acetone-d_6): δ 164.78, 160.84, 156.94, 141.28, 127.70, 124.72, 53.94. IR (ν, cm^{-1}): 1723, 1405, 1251, 1048, 764. UV-Vis absorption: λ(nm), ε (M^{-1}cm^{-1}): 252(sh, 28500), 318(63300), 393(11600), 546(15300).

Fe(bpyBr)$_3$(BF$_4$)$_2$: Yield: 90% (46 mg). ^{1}H NMR (500 MHz, MeOH-d_4): δ 9.07 (s, 6H), 7.74 (d, *J* = 4.1 Hz, 6H), 7.35 (d, *J* = 6.1 Hz, 6H). ^{13}C NMR (125 MHz, DMSO-d_6): 154.69, 150.28, 132.72, 127.24, 123.19. IR (ν, cm^{-1}): 3107, 1590, 1400, 1046, 827. UV-Vis absorption: λ(nm), ε (M^{-1}cm^{-1}): 239(59800), 292(46500), 302(54700), 358(7000), 399(3300), 497(5800), 537(6900).

$Fe(bpyMe)_3(BF_4)_2$: Yield: 80% (450 mg). ^{1}H NMR (500 MHz, MeOH-d_4): δ 8.55 (s, 6H), 7.28 (d, *J* = 6.1 Hz, 12H), 2.58 (s, 18H). ^{13}C NMR (125 MHz, acetone-d_6): δ 150.88, 144.68, 143.17, 120.02, 116.39, 11.60. IR (ν, cm^{-1}): 3077, 1618, 1444, 1029, 836. UV-Vis absorption: λ(nm), ε ($M^{-1}cm^{-1}$): 254(19900), 289(sh, 46600), 297(6000), 491(sh, 6100), 533(7100).

$Fe(bpy^tBu)_3(BF_4)_2$: Yield: 96% (2.9 g). ^{1}H NMR (500 MHz, acetone-d_6): δ 8.90 (d, *J* = 2.1 Hz, 6H), 7.57 (dd, *J* = 6.1, 2.1 Hz, 6H), 7.50 (d, *J* = 6.1 Hz, 6H), 1.40 (s, 54H). ^{13}C NMR (125 MHz, acetone-d_6): 164.50, 160.43, 154.64, 125.88, 122.44, 36.39, 30.64. IR (ν, cm^{-1}): 2955, 1614, 1220, 1026, 832. UV-Vis absorption: λ (nm), ε ($M^{-1}cm^{-1}$): 250(30500), 298(75100), 356(9300), 490(sh, 9400), 529(1100).

$Fe(bpyOMe)_3(BF_4)_2$: Yield: 87% (76 mg). ^{1}H NMR (500 MHz, MeOH-d_4): δ 8.29 (s, 6H), 7.30 (d, *J* = 6.4 Hz, 6H), 7.08 (d, *J* = 8.3 Hz, 6H), 4.03 (s, 18H). ^{13}C (125 MHz, MeOH-d_4): δ 169.66, 161.89, 155.55, 115.28, 112.06, 57.25. IR (ν, cm^{-1}): 1610, 1419, 1220, 1326, 832. UV-Vis absorption: λ (nm), ε ($M^{-1}cm^{-1}$): 279 (45000), 292(41000), 361(7000), 505(sh, 6300), 536(6400).

$Fe(bpyNH_2)_3(BF_4)_2$: Yield: 90% (713 mg). ^{1}H NMR (500 MHz, DMSO-d_6): δ 7.56 (s, 6H), 6.93 (d, *J* = 6.1 Hz, 6H), 6.77 (s, 12H), 6.67 (d, *J* = 7.8 Hz, 6H). ^{13}C NMR (125 MHz, DMSO-d_6): 157.81, 155.39, 151.66, 113.49, 107.81. IR (ν, cm^{-1}): 3369, 1615, 1497, 1018, 837.

ELECTROCHEMISTRY

Electrochemical experiments were performed with a BASi Epsilon potentiostat with the cell located in a glove box under UHP argon. All solutions were freshly prepared prior to electrochemical testing. Cyclic voltammograms were collected in a three-electrode cell consisting of a platinum wire counter electrode, freshly polished 3 mm glassy carbon working electrode, and a Ag/AgCl reference electrode. Supporting electrolyte was freshly prepared as 0.5 M solution in propylene carbonate dried over 3 Å molecular sieves.

FLOW BATTERY TESTING

Laboratory scale flow battery single cells (Fuel Cell Technologies, Albuquerque, NM) were assembled under UHP argon using 0.2 M respective catholyte and anolyte in 0.5 M supporting electrolyte in propylene carbonate dried over 3 Å molecular sieves. Peristaltic pumps (Masterflex L/S) were used to run electrolyte at a rate of 2 mL min^{-1} from polypropylene reservoirs through Norprene tubing into a serpentine 5 cm^2 flow field. Carbon felt electrodes (SGL carbon, GFD grade, 2.5 mm nominal thickness) were oxygen plasma treated with a Harrick Plasma Cleaner for 5 minutes on each carbon felt side. A Solartron 1287 potentiostat/galvanostat applied a 10-mA charge/discharge current across two carbon felt electrodes situated on opposing sides of a Fumasep FAP-450 (Fumatech) membrane and compressed to 80% of their original thickness.

Cut-off voltages for each RFB are as follows:

Symmetric $Fe(bpy)_3(BF_4)_2$ in $TEABF_4$/ $TBABF_4$/ $TBAPF_6$/ TBAOTf/ TBATFSI: 2.60 V to 2.00 V

Symmetric $Fe(bpyCF_3)_3(BF_4)_2$: 2.50 V to 1.90 V

Symmetric $Fe(bpyOMe)_3(BF_4)_2$: 2.50 V to 1.90 V

Asymmetric $Fe(bpy)_3(BF_4)_2$/$Ni(bpy)_3(BF_4)_2$: 2.60 V to 2.00 V

Asymmetric $Fe(bpyCF_3)_3(BF_4)_2$/$Ni(bpy)_3(BF_4)_2$: 3.00 V to 2.20 V

Results and Discussion

The **Samsung 1** RFB consisting of $Fe(bpy)_3(BF_4)_2$ as the 1-electron redox-active catholyte and $Ni(bpy)_3(BF_4)_2$ as the 2-electron redox-active anolyte achieved a 2.26 V battery voltage with Coulombic and voltage efficiencies of approximately 89 and 87%, respectively.[24] Though preliminary results showed acceptable Coulombic efficiency (CE) and energy efficiency (EE), the RFB exhibited irreversible capacity loss due to three main factors: high solvent crossover due to different catholyte and anolyte volumes, uncharged $Ni(0)(bpy)_3$ crossover through the anion exchange membrane, and inherent resistance of the membrane used. Studies on **Samsung 2**, the symmetric system using $Fe(bpy)_3(TFSI)_2$, showed that a symmetric RFB reduces the amount of crossover experienced between anolyte and catholyte. In an effort to optimize these

promising systems, we re-examined the cycling conditions of **Samsung 1**, and then applied them to a symmetric system like **Samsung 2**. In the optimization of **Samsung 1**, we studied anion-exchange membranes and modified the state-of-charge (SOC). These conditions were then applied in a symmetric $Fe(bpy)_3(BF_4)_2$ RFB and five supporting electrolytes were compared to find the highest performer.

One of the first factors we had to optimize was the membrane. Two common, commercial ion exchange membranes are Fumasep FAP-450 and FAP-PK, which have similar structures except FAP-PK has an additional ~30-µm thick poly(ether ether ketone) (PEEK) layer. Hudak *et al.* previously studied a variety of commercial separators and ion exchange membranes using the **Samsung 1** system and found that while the PEEK-supported membrane experienced decreased swelling that enables solvent crossover, the higher conductance of FAP-450 resulted in greater voltage efficiency.[24] We did an investigation on the **Samsung 1** system using these two membranes and collected post-cycling CVs to evaluate crossover. A comparison of the catholyte, $Fe(bpy)_3(BF_4)_2$, showed a 32.1% decrease in current using FAP-450 compared to only a 23% decrease in current with FAP-PK. The higher crossover observed for FAP-450, made it an ideal candidate to monitor active species crossover in a symmetric cell.

To find the highest performing supporting electrolyte, symmetric RFBs were assembled using FAP-450, 0.2 M $Fe(bpy)_3(BF_4)_2$ in PC, and 5 different supporting electrolytes (0.5 M). The RFBs were cycled to 80% SOC for 20 cycles; 80% SOC was selected to the commercial standard for vanadium RFBs.[28] Both the cation and anion of the supporting electrolyte were varied in these symmetric RFBs to determine which electrolyte enabled high electrochemical yield (EY), CE, VE, EE. Electrochemical yield is defined as the observed discharge capacity divided by the theoretical capacity of the cell.

Voltage, Coulombic, and energy efficiencies are summarized in Figure 1a. Over all 20 cycles, the RFB in $TEABF_4$ showed the highest efficiencies than the other 4 supporting electrolytes and an electrochemical yield 17% greater than the RFB using $TBABF_4$ (Figure 1c), where 100% EY equals 26.8 mAh. The trend in performance follows $TEABF_4$ > $TBABF_4$ > TBATFSI > $TBAPF_6$ > TBAOTf such that TEA^+ is superior to TBA^+, and BF_4^- is a superior anion with respect to all the performance metrics listed above. A comparison of ionic radius and limiting ionic conductivity shows that BF_4^- has the smallest ionic radius and highest limiting ionic conductivity, followed by PF_6^-, OTf^-, and $TFSI^-$. The cations follow the same trend: TEA^+ has a smaller ionic

radius and higher limiting ionic conductivity than TBA^+ in PC.[6] The potential vs. time plots in Figure 1b show the same trend as seen in Figure 1a: the $TEABF_4$ RFB maintained its capacity over 20 cycles and 80 hours, while the TBAOTf RFB lost capacity in half the amount of time, indicated by the shortened charge-discharge cycles.

Interestingly, the RFB in TBATFSI behaved differently throughout the 20 cycles. After reaching a low EY at cycle 4, the EY increased for 4 more cycles and then steadily decreased.[29] Post-battery cyclic voltammograms (CVs) were collected to compare un-cycled $Fe(bpy)_3(BF_4)_2$ to the cycled catholytes (**1A**) and cycled anolytes (**1A**) in each of the supporting electrolytes. CVs of the TBATFSI catholyte showed that the anolyte maintained its electrochemical profile but decreased in current density by 29%. The CV of the catholyte showed the expected profile in the first CV cyclic but showed a complete loss of redox couples in the 2nd and 3rd cycles. We believe slow anion exchange between the BF_4^- and $TFSI^-$ occurred during the first few cycles of RFB cycling and decreased the EY while the exchange took place. While the exchange was monitored by CV, low conductivity inhibited a current response at the electrode.[25] The EY then increased at cycle 5 when the anion exchange was complete. To test this, the same post-battery catholyte sample vial was allowed to sit for 2 days, after which the CV reverted to the $Fe(bpy)_3^{2+}$ redox profile. The timescale of

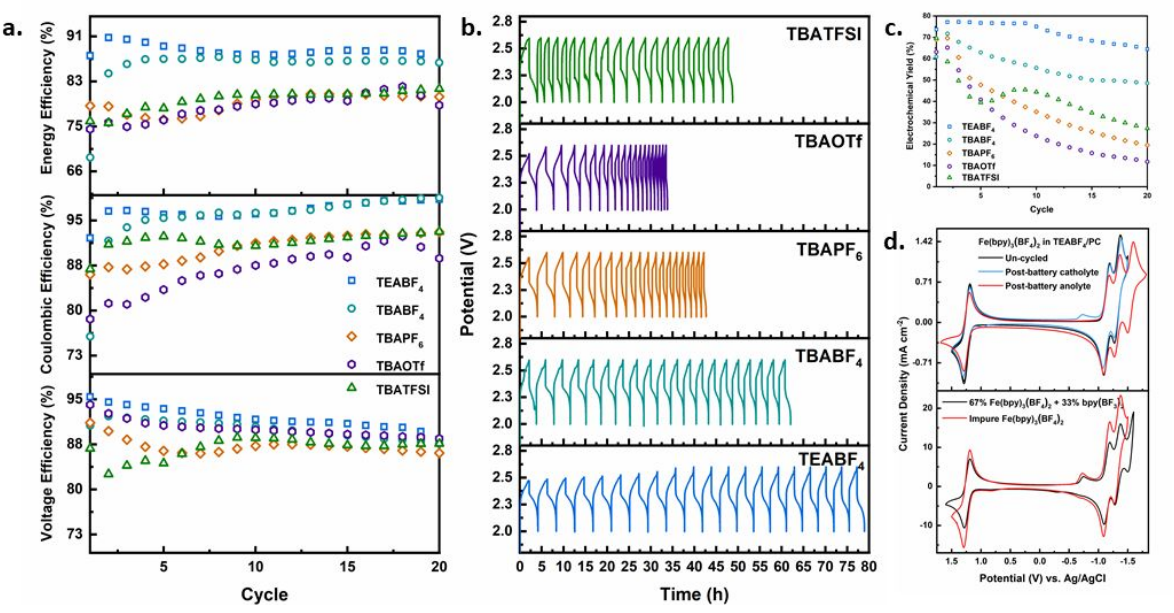

Figure 1 - a) Voltage, Coulombic, and energy efficiencies of symmetric $Fe(bpy)_3(BF_4)_2$ RFBs (0.2 M) in various supporting electrolyte salts (0.5 M) in propylene carbonate. b) Potential vs. time plots of each symmetric RFB over 20 cycles. c) Electrochemical yield of each symmetric RFB over 20 cycles. d) CVs of symmetric $Fe(bpy)_3(BF_4)_2$ (10 mM) catholyte and anolyte compared to un-cycled $Fe(bpy)_3(BF_4)_2$ (10 mM) in $TEABF_4$ (0.5 M) in propylene carbonate and overlay of an impure sample of $Fe(bpy)_3(BF_4)_2$ (10 mM) and a mixture of pure $Fe(bpy)_3(BF_4)_2$ (10 mM) with by-product, $bpy(BF_3)_2$ (10 mM) in $TEABF_4$ (0.5 M) in propylene carbonate.

the RFB showed the exchange took place over a day, while the timescale of CV was too fast to monitor the completion of the exchange in real-time.

The catholytes in all other salts showed almost no change in peak current compared to **1** (Figure S2). The anolytes of $TBABF_4$, $TBAPF_6$, and TBAOTf all showed large decreases in peak current compared to **1** (0.20 to 0.39 mA cm^{-2}, 27 to 38%), while **1A** in $TEABF_4$ showed only a small decrease (0.18 mA cm^{-2}, 21%). **1A** of TBATFSI maintained its structure but showed a large decrease in peak current compared to **1** and did not display the same anion exchange as **1C**, possibly due to the anolyte having ligand-based redox events.

Though no major changes were observed in the post-battery CVs of **1C** in each supporting electrolyte, upon re-evaluation we observed subtle new redox events occurring at -0.71 and 1.0 V, which we attribute to the formation of 1,1'-di(trifluoroborate)-2,2'-bipyridinium adduct, $bpy(BF_3)_2$. This adduct forms by the reaction of dissociated bpy in solution with hydrolyzed BF_4^- counterion.[30] Several published articles report the step-wise hydrolysis of BF_4^- to BF_3OH^-, to $BF_2(OH)_2^-$, to $BF(OH)_3^-$, a reaction that occurred from both cycling the RFB, and in the reagent bottle of $Fe(BF_4)_2{\cdot}6H_2O$ used to synthesize the complexes.[31] [32] [33] We confirmed the identity of this by-product by synthesizing $bpy(BF_3)_2$ by the reaction of bpy with 2 equivalents of BF_3 etherate, followed by characterization with ^1H NMR, CV, and mass spectrometry and comparing it to post-battery samples of the catholyte. In addition to hydrolysis during battery cycling, we found that impure $Fe(BF_4)_2{\cdot}6H_2O$ starting material used to synthesize $Fe(bpy)_3(BF_4)_2$ yielded a mixture of complex and $bpy(BF_3)_2$.

Due to the decrease in current density in post-battery anolyte CVs and the appearance of by-product peaks in the post-battery catholyte CVs, it is likely a bpy ligand of the anolyte dissociated upon charging and the negatively charged bpy migrated across the anion exchange membrane to the catholyte, where it reacted with the hydrolyzed BF_4^-. Figure 1d shows the overlay of un-cycled $Fe(bpy)_3(BF_4)_2$ and post-battery anolyte and catholyte samples. An overlay of an impure sample of $Fe(bpy)_3(BF_4)_2$ that was synthesized using hydrolyzed $Fe(BF_4)_2{\cdot}6H_2O$ starting material and a mixture of pure $Fe(bpy)_3(BF_4)_2$ and $bpy(BF_3)_2$ support the identity of the by-product formed during cycling.

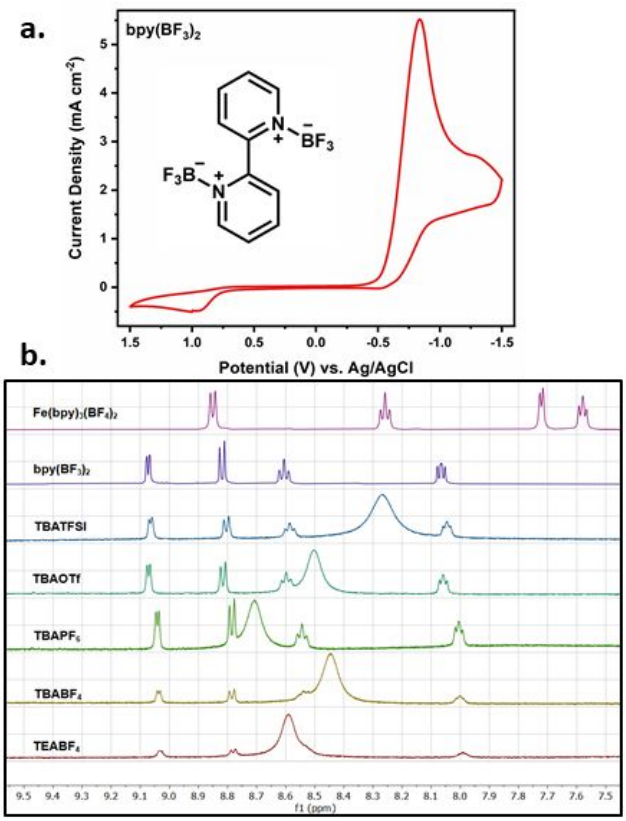

Figure 2 - a) CV of $bpy(BF_3)_2$ (10 mM) in $TEABF_4$ (0.5 M) in propylene carbonate and b) stacked ^1H NMR spectra of pure $Fe(bpy)_3(BF_4)_2$, $bpy(BF_3)_2$, and unaltered catholyte samples of RFBs with different supporting electrolyte salts (0.5 M) in propylene carbonate. ^1H NMR spectra were measured in acetone-d_6 and electrolyte, PC, and reference solvent were omitted for clarity.

Further evidence that the by-product is in the catholyte is seen in NMR spectra of unaltered samples of the post-battery catholyte, in Figure 2b. The catholyte should contain a mixture of $Fe(bpy)_3(BF_4)_2$, dissociated bpy, $bpy(BF_3)_2$, $TEABF_4$, and propylene carbonate (PC). The spectra show only $bpy(BF_3)_2$ resonances and single, broad peaks. Because the RFBs were disassembled with most of the electroactive species in the Fe^{3+} state, we see broad signals from the paramagnetic Fe^{3+} complexes, and no dissociated bpy due to stronger interactions between Fe and bpy. The amount of $bpy(BF_3)_2$ is higher in the $TBAPF_6$, TBAOTf, and TBATFSI RFBs, correlating with the lower efficiencies and EY observed. ^1H NMR spectra of the unaltered anolyte samples showed a mixture of $Fe(bpy)_3(BF_4)_2$ complex and dissociated ligand. No evidence of $bpy(BF_3)_2$ was observed, suggesting that the ligand binds to BF_3 in the catholyte. Furthermore, the peak broadening observed in the catholyte was not seen in the anolyte, due to the reduction of the anolyte occurring on the bpy. Addition of a radical onto bpy can promote ligand shedding from the Fe and

subsequent crossover into the catholyte.[34] After sitting one hour, precipitation of solids was observed in anolyte NMR samples, while catholyte samples remained in solution.

Design and Tuning of MCCs

With the goal of extending the voltage window of $Fe(bpy)_3(BF_4)_2$ in propylene carbonate, electron-withdrawing groups (EWGs) and electron-donating groups (EDGs) were introduced to the 4- and 4'-positions of 2,2'-bpy to shift the redox potentials of the $Fe^{2+/3+}$ couple.[35] Substituents with different degrees of withdrawing and donating effects were selected to cover a large redox voltage window. EWGs such as $-CF_3$ were expected to inductively pull the most electron density away from the Fe^{2+} metal center, making it more difficult to oxidize, thus shifting the potential to a higher voltage. Conversely, alkyl EDGs were expected to shift $Fe^{2+/3+}$ to more negative potentials, with respect to $Fe(bpy)_3(BF_4)_2$. The Fe-bipyridyl complexes synthesized in this study can be seen in Figure 3. All complexes were prepared by the room temperature reaction of $Fe(BF_4)_2{\cdot}6H_2O$ with bpy ligand in methanol overnight, and purity was verified using NMR.

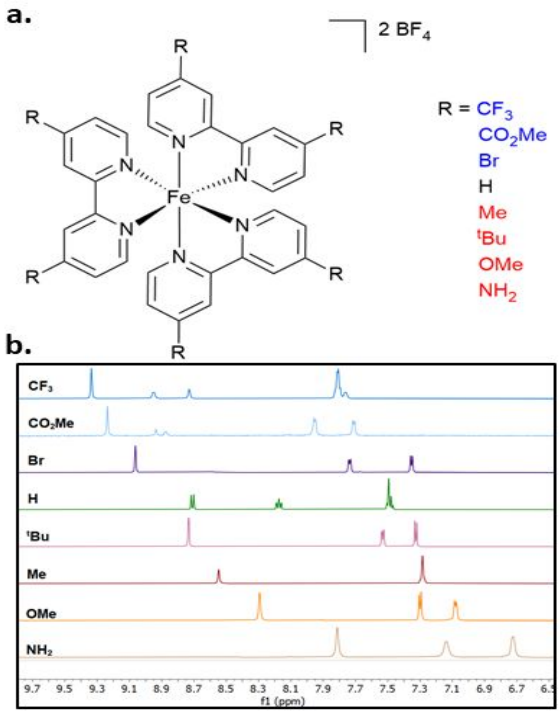

Figure 3 – a) Structure of Fe bpy complexes; electron-donating groups are shown in blue and electron-withdrawing groups are shown in red. b) ^1H NMR spectra of all complexes in methanol-d4 at room temperature; internal reference signal (3.31 ppm) and alkyl substituents are omitted for clarity.

The ^{1}H NMR spectra of the 8 iron complexes in methanol-d_4 are shown in Figure 3. An obvious trend in variable substituent is observed by the degree of deshielding observed for the bpy protons between 9.3 and 7.8 ppm. The increased electron density on the -CF_3, -CO_2Me, and -Br EWGs cause the proton resonances to shift downfield, while the opposite is observed for EDGs, with respect to the parent compound, $Fe(bpy)_3(BF_4)_2$. The top two spectra of $Fe(bpyCF_3)_3(BF_4)_2$ and $Fe(bpyCO_2Me)_3(BF_4)_2$ show additional solvent signals, indicative of ligand exchange with the solvent.[36] Methanol-d_4 was selected as the common reference solvent due to adequate solubility of all the complexes, however, while ligand exchange was mostly circumvented in methanol, it had an impact on signal splitting and coalescence of signals in both $Fe(bpy)_3(BF_4)_2$ and $Fe(bpyMe)_3(BF_4)_2$. Additionally, the spectrum of $Fe(bpyNH_2)_3(BF_4)_2$ omits the amine proton resonances due to exchange with methanol-d_4.

Absorbance and molar absorptivities were measured for each complex in propylene carbonate (Experimental and Figure S4). Little variation was observed between the iron complexes, and all exhibited π-π* and n-π* transitions from 230–350 nm, with high molar absorptivities that are characteristic of highly conjugated bipyridyl ligands. Metal-to-ligand charge transfer (MLCT) bands were observed near 500 nm and agree with literature of metal bpy complexes.[37]

Cyclic voltammograms of each of the complexes were collected in PC with an inert glassy carbon working electrode, Pt wire counter electrode, and Ag/AgCl reference electrode. First, the metal-centered $Fe^{2+/3+}$ redox couples were investigated, illustrated in Figure 4a. As expected, the most electron-withdrawing substituent resulted in positive shifts in $E_{1/2}$, achieving 1.65 V for $Fe(bpyCF_3)_3(BF_4)_2$. The redox potential for the most electron-donating substituent in solution appears for $Fe(bpyOMe)_3(BF_4)_2$ at 0.94 V. The two electron-donating alkyl groups in $Fe(bpyMe)_3(BF_4)_2$ and $Fe(bpy^tBu)_3(BF_4)_2$ show perfect overlap between redox couples, indicating that no differences in inductive effects are to be expected for similar alkyl substituents. $Fe(bpyNH_2)_3(BF_4)_2$ exhibited poor solubility in solvents of interest for RFBs; to observe its electrochemical behavior, a thin film of $Fe(bpyNH_2)_3(BF_4)_2$ in Nafion was drop-casted onto a GC electrode and measured in 0.5 M $TEABF_4$/PC (ESI). The thin film CV shows a pronounced negative shift in $E_{1/2}$ to 0.43 V, with respect to the parent $Fe(bpy)_3(BF_4)_2$. Current densities (Figure 4b) are comparable for all complexes

(10 mM), however $Fe(bpyMe)_3(BF_4)_2$ showed a slight increase while $Fe(bpyOMe)_3(BF_4)_2$ exhibited decreased current density.

Table 1 summarizes $E_{1/2}$ for each redox species: $Fe^{2+/3+}$ couple, ligand-centered $[Fe(bpyR)_3]^{2+/+}$, voltage separation between these two redox events, and diffusion coefficients. The voltage separation (column ΔE_{RFB}) shows that as the complexes were cycled across the solvent window to observe battery voltage, ligand-based redox events shifted together with the $Fe^{2+/3+}$ redox event. Theoretical battery voltages ranged between 2.21 and 2.37 V, where $Fe(bpy)_3(BF_4)_2$ achieves the greatest voltage. Ligand-centered redox events were not reported for $Fe(bpyBr)_3(BF_4)_2$ due to ligand dissociation upon negative sweep. CVs performed on the solution after resting for 3 days showed re-association of the ligands and reversibility of the $Fe^{2+/3+}$ redox couple. The $Fe(bpyNH_2)_3(BF_4)_2$ thin film shows irreversible redox peaks at negative potentials and almost immediate delamination of the thin film.

Table 1 – Redox potentials and diffusion coefficients of all Fe bpy complexes.

	$[Fe(bpyR)_3]^{3+/2+}$ $E_{1/2}$ (V)[a]	$[Fe(bpyR)_3]^{2+/+}$ $E_{1/2}$ (V)	ΔE_{RFB} (V)	$[Fe(bpyR)_3]^{3+/2+}$ Diff. Coeff. ($cm^2\ s^{-1}$)	$[Fe(bpyR)_3]^{2+/+}$ Diff. Coeff. ($cm^2\ s^{-1}$)
$Fe(bpyCF_3)_3(BF_4)_2$	1.65	-0.63	2.28	6.14×10^{-7}	5.49×10^{-7}
$Fe(bpyCO_2Me)_3(BF_4)_2$	1.53	-0.68	2.21	4.49×10^{-7}	4.44×10^{-7}
$Fe(bpyBr)_3(BF_4)_2$	1.43	-	-	7.07×10^{-8} [b]	-
$Fe(bpy)_3(BF_4)_2$	1.25	-1.12	2.37	1.12×10^{-6}	8.90×10^{-7}
$Fe(bpy^tBu)_3(BF_4)_2$	1.09	-1.19	2.28	4.91×10^{-7}	-
$Fe(bpyMe)_3(BF_4)_2$	1.07	-1.25	2.32	8.76×10^{-7}	7.62×10^{-7}
$Fe(bpyOMe)_3(BF_4)_2$	0.94	-1.27	2.21	4.97×10^{-7}	6.21×10^{-7}

$[Fe(bpyR)_3]^{3+/2+}$ $E_{1/2}$ is the redox potential of this redox couple; $[Fe(bpyR)_3]^{2+/+}$ $E_{1/2}$ is the redox potential of this redox couple; ΔE_{RFB} is the separation between $[Fe(bpyR)_3]^{3+/2+}$ $E_{1/2}$ and $[Fe(bpyR)_3]^{2+/+}$ $E_{1/2}$; the diffusion coefficients were calculated for each of the respective redox couples. Standard redox potentials (measured vs. Ag/AgCl) identified using cyclic voltammetry from 25 to 500 mV s^{-1}, of Fe complex (10 mM) in $TEABF_4$/PC (0.5 M).

Electrochemical reversibility was determined by CVs collected at scan rates ranging from 25 to 500 mV s^{-1}, of both the anolyte and catholyte sides of the complexes. Diffusion coefficients were calculated using the Randles-Sevcik equation for reversible redox processes, listed in Table 1, and all exhibit comparable diffusion to other reported $Fe(bpy)_3^{2+}$ complexes.[23] [36] Figure 5 shows the reversibility and linearity of $Fe(bpyCF_3)_3(BF_4)_2$, indicating that the redox events are diffusion-controlled processes. Furthermore, both

the anolyte and catholyte reductions show similar diffusion coefficients, indicating that both species experience the same mobility in the catholyte and anolyte.

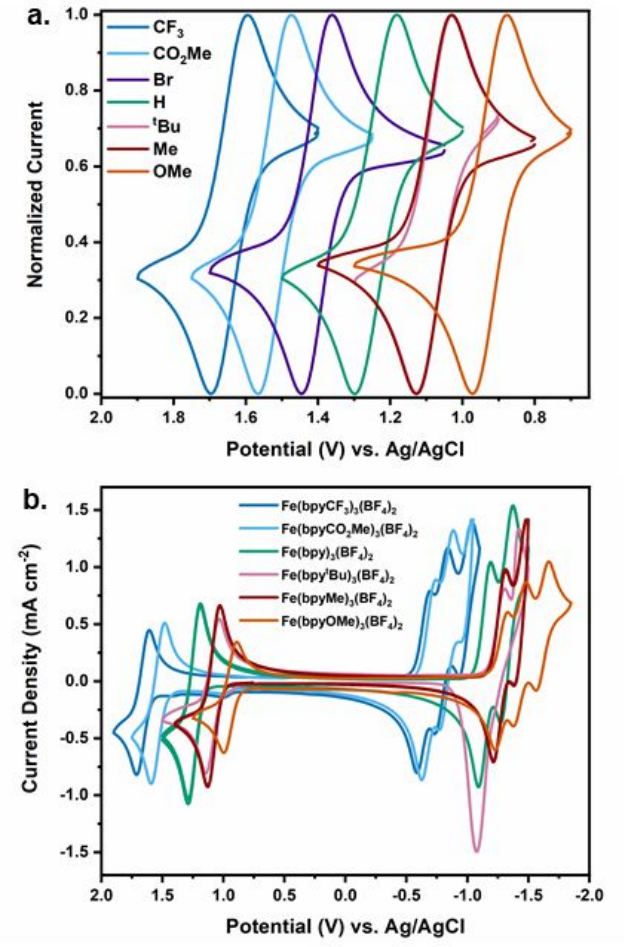

Figure 5 – Cyclic voltammograms of a) $Fe^{2+/3+}$ and b) full redox window of Fe bpy complexes (10 mM) measured in $TEABF_4$/PC (0.5 M) using a glassy carbon working electrode, Pt wire counter electrode, and Ag/AgCl reference electrode at room temperature, collected at 100 mV s^{-1}. $Fe(bpyBr)_3(BF_4)_2$ is omitted from b for clarity.

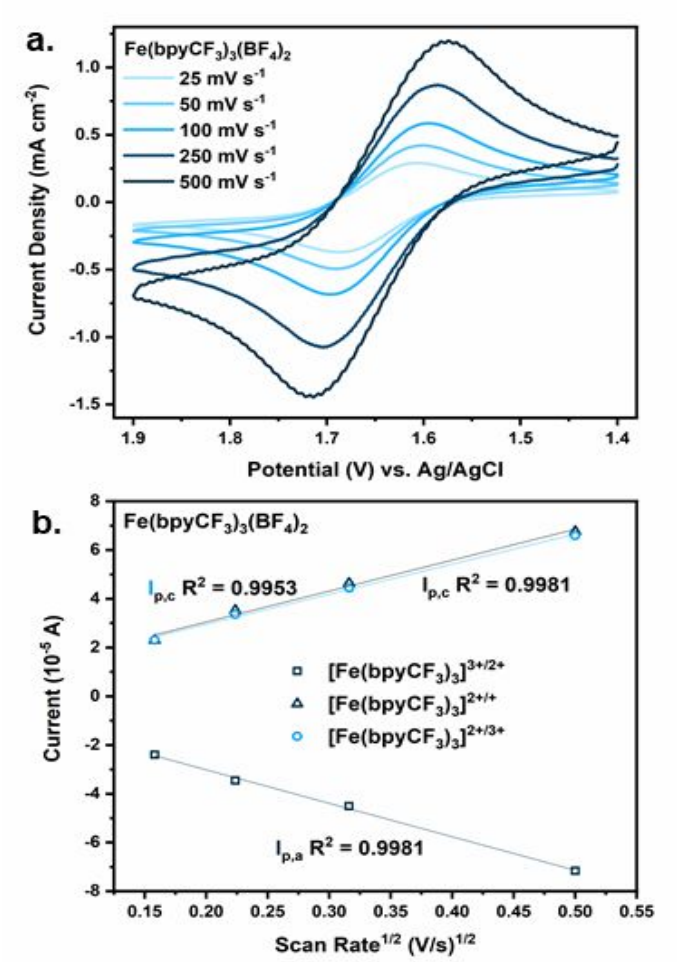

Figure 4 – Scan rate dependence of $Fe(bpyCF_3)_3(BF_4)_2$.

New Fe Complexes for Symmetric RFBs

Two of the newly synthesized complexes, $Fe(bpyCF_3)_3(BF_4)_2$ and $Fe(bpyOMe)_3(BF_4)_2$, were studied in lab-scale RFBs using the optimized conditions discussed above to understand the effect ligand inductive effects have on RFB performance compared to unsubstituted $Fe(bpy)_3(BF_4)_2$. The results summarized in Figure 6 show that while efficiencies of each are comparable, their capacities are vastly different. The unsubstituted

complex achieved the highest EY over 20 cycles, with an average EY 62% higher than $Fe(bpyOMe)_3(BF_4)_2$ and 88% higher than $Fe(bpyCF_3)_3(BF_4)_2$. Upon disassembling the $Fe(bpyCF_3)_3(BF_4)_2$ RFB, the anolyte reservoir showed precipitation and very little solvent. Post-cycling analysis was performed on the symmetric RFBs to understand what factors were detrimental to performance. CVs of $Fe(bpyCF_3)_3(BF_4)_2$ and $Fe(bpyOMe)_3(BF_4)_2$ catholytes and anolytes showed no obvious complex degradation, and no electrochemically active by-product formation. $Fe(bpyCF_3)_3(BF_4)_3$ catholyte and anolyte both showed decreases in current density of 17 and 31%, respectively. $Fe(bpyOMe)_3(BF_4)_2$ catholyte showed a large increase in current relative to the un-cycled complex, while the anolyte showed only a slight increase.

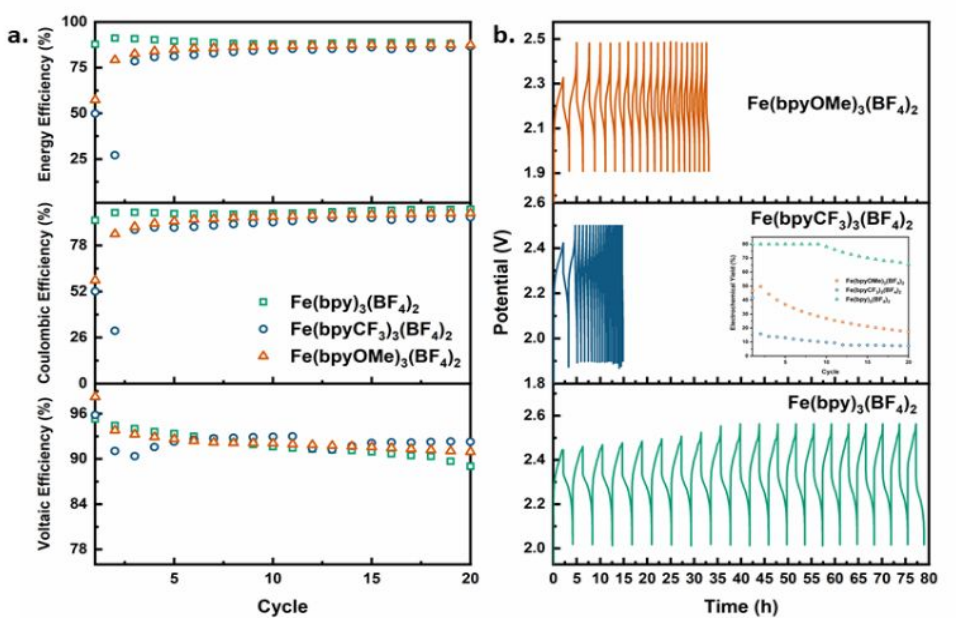

Figure 6 - a) Voltage, Coulombic, and energy efficiencies of symmetric $Fe(bpyCF_3)_3(BF_4)_2$, $Fe(bpy)_3(BF_4)_2$, and $Fe(bpyOMe)_3(BF_4)_2$ RFBs (0.2 M) in $TEABF_4$ (0.5 M) in propylene carbonate, and b) potential vs. time plots of each RFB. Inset: EY of each battery.

^{1}H NMR analysis of $Fe(bpyCF_3)_3(BF_4)_2$ extracts showed catholyte complex, dissociated $bpyCF_3$, and no evidence of by-products, however, the anolyte spectrum only displayed ligand resonances, indicating that the complex completely dissociated during cycling and Fe may have precipitated from solution. Preparation of a sample solution of the precipitate for NMR yielded a soluble product that displayed $Fe(bpyCF_3)_3(BF_4)_2$ and ligand resonances in the spectrum, leading us to believe that the precipitated product could be easily re-coordinated to form the MCC. Spectra of $Fe(bpyOMe)_3(BF_4)_2$ showed that both the catholyte and anolyte remained unchanged throughout cycling. Furthermore, while the un-cycled complex and catholyte spectra showed some dissociated ligand resonances, the anolyte did not. This could be due to ligand shedding during cycling and subsequent crossover into the catholyte that also contributed to abnormally high current densities post-cycling.

MALDI-MS analysis on the $Fe(bpyCF_3)_3(BF_4)_2$ catholyte and anolyte supported the NMR results: the catholyte sample showed presence of complex and dissociated $bpyCF_3$ ligand, while the anolyte sample showed no evidence of $Fe(bpyCF_3)_3(BF_4)_2$. $BpyCF_3$ dominated the anolyte signal and evidence of partially hydrolyzed ligand in the form $bpy(CF_3)(CF_2OH)$ was present.

A Higher Voltage Asymmetric RFB

The complex with the highest potential redox event, $Fe(bpyCF_3)_3(BF_4)_2$, was chosen to analyze its stability as a high voltage asymmetric RFB. First, an asymmetric system was assembled to establish baseline performance, using the conditions established for the symmetric RFBs discussed above. $Fe(bpy)_3(BF_4)_2$ was chosen as the catholyte and $Ni(bpy)_3(BF_4)_2$ as the anolyte for the **Optimized** RFB. Fe experiences a 1-electron redox event and Ni experiences a 2-electron redox couple, so 0.2 M solutions of each electroactive species in $TEABF_4$/PC (0.5 M) were prepared: 5 mL of catholyte and 10 mL of anolyte. Using the same concentrations in different volumes was necessary to maintain similar ionic strengths, limit crossover due to diffusion,[24] and match capacities of the catholyte and anolyte. Average voltage, Coulombic, and energy efficiencies of **Optimized** were 90.7%, 80.7%, and 89.0%, respectively. Cycles 1-6 remained relatively steady while cycles 7-11 showed a decrease in both CE and EE before increasing and stabilizing for the remaining cycles (Figure 7a). While the CE of **Optimized** did not surpass that of **Samsung 1** (90.4%), the EE increased by 7.2%.

With conditions for an asymmetric RFB established, the complex with the highest potential redox event, $Fe(bpyCF_3)_3(BF_4)_2$, was chosen as the catholyte to study against 3 different anolytes. The anolyte species selected were: $Ni(bpy)_3(BF_4)_2$ to understand the effect of catholyte modification on battery performance; $Fe(bpy)_3(BF_4)_2$ because the symmetric RFB had the highest capacity of other symmetric systems studied; and $FcBF_4$ as an established, reversible electrochemical compound.

Our **Next Gen** RFB was prepared using $Fe(bpyCF_3)_3(BF_4)_2$ as the high potential catholyte and $Ni(bpy)_3(BF_4)_2$ as the anolyte to produce a RFB with a theoretical voltage of 2.66 V. **Next Gen** was cycled 20 times after which it achieved an average VE, CE, and EE of 94.1%, 90.6%, and 78.0%, respectively. The EY was 20% lower than **Optimized** by the 20th cycle, equivalent to capacity fade of 86% vs. 66% for **Optimized**.

Post-battery analysis of the catholyte by CV showed a slight distortion in the redox profile but maintained its electrochemical reversibility, however, current density decreased by 50% compared to the un-cycled complex. NMR spectra collected on the unaltered catholyte sample (Figure 7d) showed peaks for $Fe(bpyCF_3)_3(BF_4)_2$ and dissociated $bpyCF_3$, and a small amount of $Fe(bpy)_3(BF_4)_2$. The CV of the anolyte, on the other hand, showed the formation of two new irreversible oxidation events at different voltages than

the un-cycled $Ni(bpy)_3(BF_4)_2$, indicating complex degradation occurred during cycling. Furthermore, inspection of the anolyte solution post-cycling revealed a change in color and precipitate formation. Exposure of the anolyte to air reverted the color back from brown to red, most likely due to oxidation of Ni^0 back to Ni^{2+}. Complex degradation is not uncommon in the field of flow batteries and cyclability has shown to suffer in high voltage systems due to complex degradation which usually leads to capacity fade.[38] Mass spectra of the anolyte only showed peaks for bpy, a small amount of $bpy(BF_3)_2$, and no complex, confirming complex degradation. Mass spectra of the catholyte was too low concentration to accurately detect the complex, but the $bpy(BF_3)_2$ by-product formed from $Ni(bpy)_3(BF_4)_2$ degradation was present, as well as $bpy(CF_3)(CF_2OH)$.

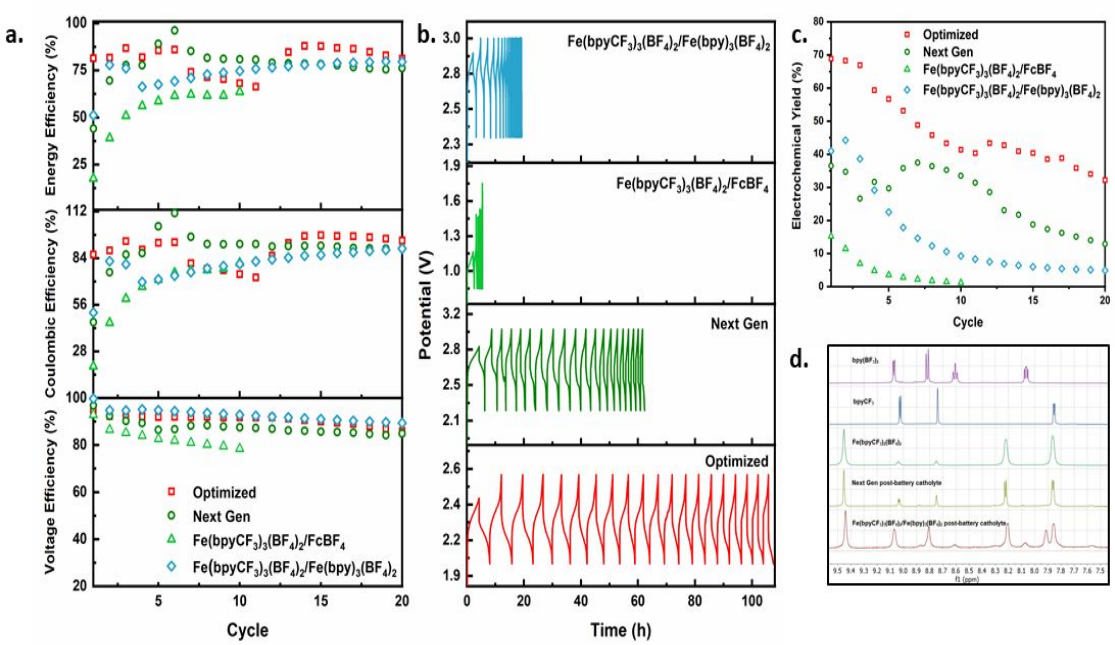

Figure 7 - a) VE, CE, and EE of the 4 asymmetric RFBs, b) potential vs. time plots of each asymmetric RFB, c) change in EY over 20 cycles, and d) ^1H NMR comparison of $Fe(bpyCF_3)_3(BF_4)_2$, post-cycling catholytes, and the catholyte components.

$Fe(bpyCF_3)_3(BF_4)_2$ was cycled with $FcBF_4$ and $Fe(bpy)_3(BF_4)_2$ as the anolytes in 2 other RFBs. $FcBF_4$ diffused across the anion exchange membrane throughout cycling and the RFB showed no capacity (Figure 7b). An H-cell experiment was performed under the same flow cell conditions to verify this diffusion process, and within a few hours, visible volume changes were observed from diffusion of the anolyte to the catholyte. NMR spectra were not collected on the catholyte and anolyte due to the paramagnetic nature of $FcBF_4$. The

RFB studied using $Fe(bpy)_3(BF_4)_2$ as the anolyte showed a quick decrease in EY, dropping from 41 to 5% over the 20 cycles. Post-cycling CVs of the catholyte showed 4 redox couples from 1.25 to 1.69 V, where the highest potential couple is attributed to $Fe(bpyCF_3)_3(BF_4)_2$ and the lowest appears due to $Fe(bpy)_3(BF_4)_2$ that crossed the membrane to the catholyte. The ^1H NMR spectrum of the catholyte showed a mixture of products: $Fe(bpyCF_3)_3(BF_4)_2$, dissociated $bpyCF_3$, some small peaks of $bpy(BF_3)_2$, and small amounts of $Fe(bpy)_3(BF_4)_2$. Any evidence of $bpy(BF_3)_2$ and $bpyCF_3$ ligand redox couples in the CV would have been obscured by the catholyte and anolyte redox events. $BpyCF_3$ is electrochemically active, with a reversible redox couple in 0.5 M $TEABF_4$/PC at -1.45 V vs. Ag/AgCl, but this peak also overlaps with anolyte redox couples present in the sample. Post-cycling electrochemical analysis of the anolyte showed less resolved negative redox couples and a decrease in current density of 53%. The NMR spectrum showed a mixture of complex, dissociated bpy, and surprisingly, $bpyCF_3$ from the catholyte. As mentioned above, though anion exchange membranes effectively prevent cation crossover, neutral compounds have crossed the membrane.[24]

In an effort to quantify the change in concentration of catholytes and anolytes post-cycling, UV-Vis spectroscopy was performed. To our surprise, the calculations resulted in vast increases greater than the starting 0.2 M. These data suggest that other by-products that were not observed by CV, NMR, or MS are present and result in abnormally high absorbance values that prevent accurate estimation of battery concentration.

Conclusions

In this paper we sought to improve upon the seminal non-aqueous RFB by Mun *et al.* by focusing on the voltage optimization of the **Samsung 1** system. We evaluated 3 symmetric RFBs with varying electronic properties to understand how modified non-innocent ligands affected battery cycling. We found that unsubstituted $Fe(bpy)_3(BF_4)_2$ produced the best battery, with good efficiencies and superior capacity to the other symmetric systems. The counterion, however, proved detrimental to complex stability, and contributed to the formation of an irreversible by-product during cycling.

With the goal of producing a higher voltage RFB than the symmetric cells, the highest potential catholyte was paired with 3 different anolytes to evaluate its stability and viability in asymmetric systems. Capacity of all 3 systems proved poor and chemical degradation mainly originated in the anolytes. Excluding evidence of hydrolysis of dissociated bpyCF_3 ligands, the anticipated catholyte degradation was not observed in **Next Gen**. This side-by-side comparison of symmetric and asymmetric systems is the first of its kind, to the best of our knowledge. In all cases, the anolyte solubilities decreased upon reduction, resulting in precipitation of active species and decreased EY.

In summary, **Optimized** outperformed the other 3 asymmetric RFBs in EY and efficiencies. **Next Gen** showed decent performance, following closely behind **Optimized** in efficiency, but showed decreased capacity and a significant decrease in current after cycling. CV, NMR, and MS analyses helped to elucidate the products formed during battery cycling, indicating that Fe and Ni bpy MCCs are unstable as anolytes in RFBs. The unsubstituted $Fe(bpy)_3(BF_4)_2$ complex resulted in the highest EY of all RFBs studied and maintained its structure and performance as a catholyte throughout cycling. The electronically modified catholytes were destabilized with new substituents which impacted their practicality as next generation catholytes. Fe MCCs having ligand-centered redox events would require increased complexation stability to prevent ligand dissociation to function as effective anolytes. Future studies on stable organic anolytes may complement $Fe(bpy)_3(BF_4)_2$ to make a high-voltage and stable RFB.

Conflicts of interest

There are no conflicts to declare.

Acknowledgements

This work was generously supported by program manager Dr. Imre Gyuk through the U.S. Department of Energy, Office of Electricity. Sandia National Laboratories is a multi-mission laboratory managed and operated by National Technology and Engineering Solutions of Sandia, LLC., a wholly owned subsidiary of Honeywell International, Inc., for the U.S. Department of Energy's National Nuclear Security Administration

under contract DE-NA0003525. The views expressed in this article do not necessarily represent the views of the U.S. Department of Energy or the United States Government.

Notes and references

‡ Matson *et al*. have been instrumental in studying polyoxovanadium clusters as viable options for non-aqueous redox flow batteries. See L. E. VanGelder, A. M. Kosswattaarachchi, P. L. Forrestel, T. R. Cook, E. M. Matson. *Chem. Sci.* 2018, **9**, 1692.

1 W. Wang, Q. Luo, B. Li, X. Wei, L. Li, Z. Yang. *Adv. Funct. Mater.* 2013, **23**, 970.

2 L. F. Arenas, C. Ponce de León, F. C. Walsh. *Curr. Opin. Electrochem.* 2019, **16**, 117.

3 Z. Yang, J. Zhang, M. C. W. Kintner-Meyer, X. Lu, D. Choi, J. P. Lemmon, J. Liu. *Chem. Rev.* 2011, **111**, 3577.

4 B. Dunn, H. Kamath, J.-M. Tarascon. *Science*, 2011, **334**, 928.

5 Y. Huang, S. Gu, Y. Yan, S. F. Y. Li. *Curr. Opin. Chem. Eng.* 2015, **8**, 105.

6 K. Gong, Q. Fang, S. Gu, S. F. Y. Li, Y. Yan. *Energy Environ. Sci.* 2015, **8**, 3515.

7 A. Z. Weber, M. M. Mench, J. P. Meyers, P. N. Ross, J. T. Gostick, Q. Liu. *J. Appl. Electrochem.* 2011, **41**, 1137.

8 J.-H. Kim, S. Ryu, S. Maurya, J.-Y. Lee, K.-W. Sung, J.-S. Lee, S.-H. Moon. *RSC Adv.* 2020, **10**, 5010.

9 S. on Tung, S. L. Fisher, N. A. Kotov, L. T. Thompson. *Nat. Commun.* 2018, **9**, 1.

10 R. A. Potash, J. R. McKone, S. Conte, H. D. Abruña. *J. Electrochem. Soc.* 2016, **163**, A338.

11 T. M. Anderson, D. Ingersoll, A. J. Rose, C. L. Staiger, J. C. Leonard. *Dalt. Trans.* 2010, **39**, 8609.

12 H. D. Pratt, J. C. Leonard, L. A. M. Steele, C. L. Staiger, T. M. Anderson. *Inorganica Chim. Acta* 2013, **396**, 78.

13 Y. Li, P. Geysens, X. Zhang, J. Sniekers, J. Fransaer, K. Binnemans, I. F. J. Vankelecom. *J. Power Sources* 2020, **450**, 227634.

14 Y. Zhen, C. Zhang, J. Yuan, Y. Zhao, Y. Li. *J. Power Sources* 2020, **445**, 227331.

15 I. L. Escalante-García, J. S. Wainright, L. T. Thompson, R. F. Savinell. *J. Electrochem. Soc.* 2015, **162**, A363.

16 J. D. Saraidaridis, B. M. Bartlett, C. W. Monroe. *J. Electrochem. Soc.* 2016, **163**, A1239.

17 J. A. Suttil, J. F. Kucharyson, I. L. Escalante-Garcia, P. J. Cabrera, B. R. James, R. F. Savinell, M. S. Sanford, L. T. Thompson. *J. Mater. Chem. A* 2015, **3**, 7929.

18 T. Chu, I. A. Popov, G. A. Andrade, S. Maurya, P. Yang, E. R. Batista, B. L. Scott, R. Mukundan, B. L. Davis. *ChemSusChem,* 2019, **12**, 1304.

19 H. S. Kim, T. Yoon, J. Jang, J. Mun, H. Park, J. H. Ryu, S. M. Oh. *J. Power Sources*, 2015, **283**, 300.

20 R. W. Hogue, C. G. Armstrong, K. E. Toghill. *ChemSusChem*, 2019, **12**, 4506.

21 C. G. Armstrong, K. E. Toghill. *J. Power Sources*, 2017, **349**, 121.

22 R. W. Hogue, K. E. Toghill. *Curr. Opin. Electrochem.* 2019, **18**, 37.

23 J. Mun, M.-J. Lee, J.-W. Park, D.-J. Oh, D.-Y. Lee, S.-G. Doo. *Electrochem. Solid-State Lett.* 2012, **15**, A80.

24 N. S. Hudak, L. J. Small, H. D. Pratt, T. M. Anderson. *J. Electrochem. Soc.* 2015, **162**, A2188.

25 J. Mun, D.-J. Oh, M. S. Park, O. Kwon, H.-T. Kim, S. Jeong, Y. G. Kim, M.-J. Lee. *J. Electrochem. Soc.* 2018, **165**, A215.

26 D. Miyoshi, H. Karimata, Z.-M. Wang, K. Koumoto, N. Sugimoto. *J. Am. Chem. Soc.* 2007, **129,** 5919.

27 Ł. Skórka, M. Filapek, L. Zur, J. G. Małecki, W. Pisarski, M. Olejnik, W. Danikiewicz, S. Krompiec. *J. Phys. Chem. C,* 2016, 120, 7284.

28 L. Li, S. Kim, W. Wang, M. Vijayakumar, Z. Nie, B. Chen, J. Zhang, G. Xia, J. Hu, G. Graff, J. Liu, Z. Yang. *Adv. Energy Mater.* 2011, **1**, 394.

29 X. Wang, X. Xing, Y. Huo, Y. Zhao, Y. Li, H. Chen. *Int. J. Electrochem. Sci.* 2018, **13**, 6676.

30 E. V. Carino, C. E. Diesendruck, J. S. Moore, L. A. Curtiss, R. S. Assary, F. R. Brushett. *RSC Adv.* 2015, **5**, 18822.

31 R. E. Mesmer, K. M. Palen, C. F. Baes Jr. *Inorg. Chem.* 1973, **12**, 89.

32 M. Anbar, S. Guttmann. *J. Phys. Chem.* 1960, **64**, 1896.

33 C. A. Wamser. *J. Am. Chem. Soc.* 1948, **70**, 1209.

34 C. S. Sevov, S. L. Fisher, L. T. Thompson, M. S. Sanford. *J. Am. Chem. Soc.* 2016, **138**, 15378.

35 J. P. Nolan, T. W. Jones, S. W. Donne, G. J. Wilson. *Electrochim. Acta,* 2013, **108**, 690.

36 Y.-W. D. Chen, K. S. Santhanam, A. J. Bard. *J. Electrochem. Soc.* 1981, **128**, 1460.

37 P. S. Braterman, J.-I. Song, R. D. Peacock. *Inorg. Chem.* 1992, **31**, 555.

38 A. Parasuraman, T. M. Lim, C. Menictas, M. Skyllas-Kazacos. *Electrochim. Acta,* 2013, **101**, 27.

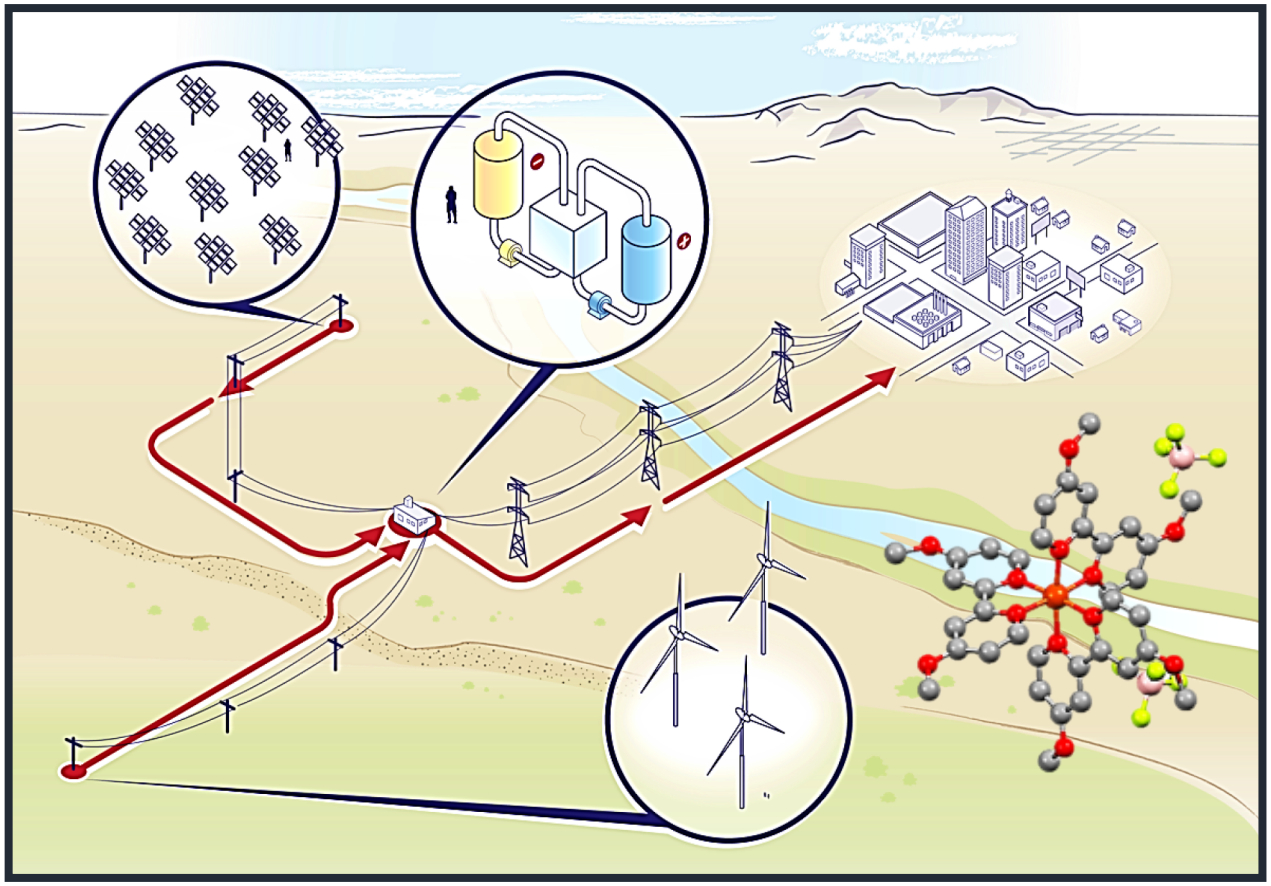

A new family of tunable iron bipyridine coordination complexes has been synthesized and tested in a non-aqueous flow battery.